Proceedings of the 25th International Conference on
Port and Ocean Engineering under Arctic Conditions
June 9-13, 2019, Delft, The Netherlands

Experiments on the Micromechanics of Ice using Scanning Electron Microscopy

Mark W Shortt[1], Peter R Sammonds[1]
[1] Institute for Risk and Disaster Reduction (University College London, London, UK)

ABSTRACT

From both geophysical and engineering perspectives, a comprehensive characterisation of the micromechanical behaviour of ice is desirable. The deformation of ice observed on larger scales, both in the field and laboratory, is controlled by the underlying microstructure of the ice, as well as internal defects incorporated into the microstructure. Thus, to fully understand the deformation behaviour of the sea ice cover across the Arctic Basin, or at a more local scale, interactions between sea ice floes and offshore structures, knowledge of the microstructure of the ice, and its micromechanical response under applied stresses are imperative. We have developed an experimental methodology for in-situ mechanical testing of millimetre-scale ice samples within the chamber of a scanning electron microscope (SEM). This enables the measurement of the stress-strain behaviour of the ice as well as simultaneous real-time imaging of the surface topography, providing a visual indication of the micromechanical processes occurring during deformation. In this paper, we give a description of the experimental methodology, followed by results from preliminary compression tests on freshwater ice samples. Prior to testing, the surface of each sample was imaged, revealing microstructural features such as grain boundaries. Stress-strain curves were obtained for each test in addition to videos of the SEM display during deformation. The SEM imaging revealed various deformation features during the tests, most notably crack initiation and propagation and the eventual failure of the samples. Applying this methodology to saline ice, in conjunction with concurrent mechanical tests on larger scales, we aim to establish empirical scaling relations for sea ice mechanics. These results may then be implemented into basin-scale sea ice models as well as models for ice-structure interactions.

KEY WORDS: Ice; Micromechanics; Scanning Electron Microscopy; Scaling

INTRODUCTION

A knowledge of the mechanics of ice is important from both geophysical and engineering perspectives. In the former case, large-scale sea ice fracturing and lead formation plays an important role in the exchange of energy and momentum between the ocean and atmosphere, whilst flow dynamics in polar ice sheets are of interest in modelling future sea level rise. In the case of engineering, a thorough characterisation of the mechanical properties of sea ice is necessary for design considerations in Arctic offshore structures and shipping.

The mechanical behaviours observed in the laboratory, and on larger scales encountered in the field are a consequence of underlying micromechanical processes. In nature, ice occurs as a polycrystalline material, with the observed bulk behaviour occurring as a large-scale manifestation of interactions between individual ice grains on the microscale [*Sammonds et al.*, 2017)]. Therefore, to fully describe observations occurring on larger scales it is necessary to understand the fundamental micromechanics of ice. Furthermore, with a sufficient knowledge of the micromechanics, it is possible to develop scaling laws for key mechanical properties in ice [e.g. *Weiss,* 2001; *Weiss and Dansereau*, 2017],

In sea ice, an important process governing the mechanical behaviour of thick sea ice features (ridging and rafting) is the degree of freeze-bonding. The temporal development of freeze-bond strength, and its dependence on physical parameters such as salinity and temperature, are essential in governing the initial strength of a thick sea ice feature. For example, if we assume the rubble in a ridge keel to behave as a Mohr-Coulomb material, the freeze-bond strength can be seen as analogous to the cohesion, which gradually increases with depth as the keel consolidates. Thus, the freeze-bond strength is an important input parameter in load calculations for ice-structure interactions [*ISO19906*]. Freeze-bonding also plays a role in determining the resistance encountered by Arctic-dwelling vessels in brash ice channels. There have been a number of previous studies on the mechanics of freeze-bonds [e.g. *Ettema and Schaefer*, 1986; *Shafrova and Høyland,* 2008; *Repetto-Llamazares et al.*, 2011; *Bailey et al.*, 2012] However, to date experiments on the micromechanical behaviour of freeze-bonds have yet to be conducted.

Scanning electron microscopy is a common method of imaging in material sciences in which the surface topography of a sample is deduced via characteristic interactions with incoming electrons. Whilst there have numerous studies on SEM imaging of ice [e.g. *Cross*, 1969; *Barnes et al.*, 2002], there has been very little research on the in-situ deformation of ice under the SEM. *Schulson et al.* (1989) conducted fracture experiments on freshwater polycrystalline ice in-situ using scanning electron microscopy. They found that samples failed via transgranular cleavage, with pores acting as initiation sites for cleavage steps. To our knowledge, no further research has been conducted on the in-situ deformation of ice using scanning electron microscopy.

In this paper, we describe a methodology that has been developed to conduct deformation testing on millimetre-scale ice samples in-situ under a scanning electron microscope. This enables the determination of the underlying micromechanical processes occurring during deformation. The results from six practice tests on dummy ice samples are detailed: four level ice, and two freeze-bonded ice.

METHODOLOGY

Experimental Set-Up

The experiments were conducted in the UCL Scanning Electron Microscope (SEM) Laboratory over a four-day period. The laboratory contains a Jeol JSM-6480LV high-performance, large volume, variable pressure analytical scanning electron microscope, with a maximum resolution of 3.0 nm. The SEM comprises an electron gun, producing a focused, collimated beam of electrons directed towards a sample. The energy E (in eV) of the electrons is proportional to the accelerating voltage V, and can be equated to the electronic kinetic energy via the following relation:

$$E = eV = \frac{1}{2} m_e v^2 \tag{1}$$

where e is the electronic charge, m_e is the electron rest mass and v is the velocity of electron. The atoms in the sample interact with the incoming electrons and produce signals which characterise its surface topography. For surface imaging purposes, the SEM contains two methods of detection, which distinguish two types of physical interaction mechanisms: secondary electron (high vacuum) and backscattered electron (low vacuum). In the tests described in this paper, high vacuum (secondary electron) mode was primarily used with the aim of obtaining higher resolution images.

In-situ deformation is possible using a Deben Microtest deformation stage (MT10114), which is placed beneath the electron gun inside the SEM chamber. A milimetre-scale sample is placed between two sets of jaws with extension measured using an extensometer and applied load via a 5 kN load cell. Both parameters are measured real-time at a sampling interval of up to 100 ms. By changing the jaws, the Microtest stage is capable of conducting compression, tensile and 3-point bending tests (only compression is described here) at motor-speeds between 0.05-1.6 mm/min. The major components of the Deben Microtest stage are shown in Figure 1.

The Microtest stage is cooled to subzero temperatures via a circulation of supercooled nitrogen gas that passes through each jaw. Nitrogen gas, originating from a pressurized cylinder, is circulated through tubes at a pressure of 7.5 psi. The gas is first passed through a dewar of liquid nitrogen to enable supercooling. Following this, the gas is separated into two closed loops, one for each jaw, passing through the SEM chamber via a set of connections on a custom SEM door. The exhausted gas is then passed back into liquid nitrogen dewar, providing further cooling for the incoming gas. The temperature of the stage is measured by an individual k-type thermocouple and displayed via a Gatan HTC2 controller. The temperature of the stage can be set to a desired value using the Gatan HTC2 controller in parallel with a Xantrex HPD 60-5 variable DC power supply, which provides an appropriate amount of heat required to keep the stage at a constant temperature. The overall test set-up is shown in Figure 2.

The shortest sampling interval for imaging under the SEM is 20 seconds, which poses difficulty when trying to image dynamic changes to the sample during the deformation. This was rectified by using a video capture card connected to the VGA output of the desktop computer used to operate the SEM. The SEM software contains a real-time view of the sample under the SEM, which was mirrored onto a separate laptop computer and recorded using video capture software at a frame rate of 60 frames-per-second (fps).

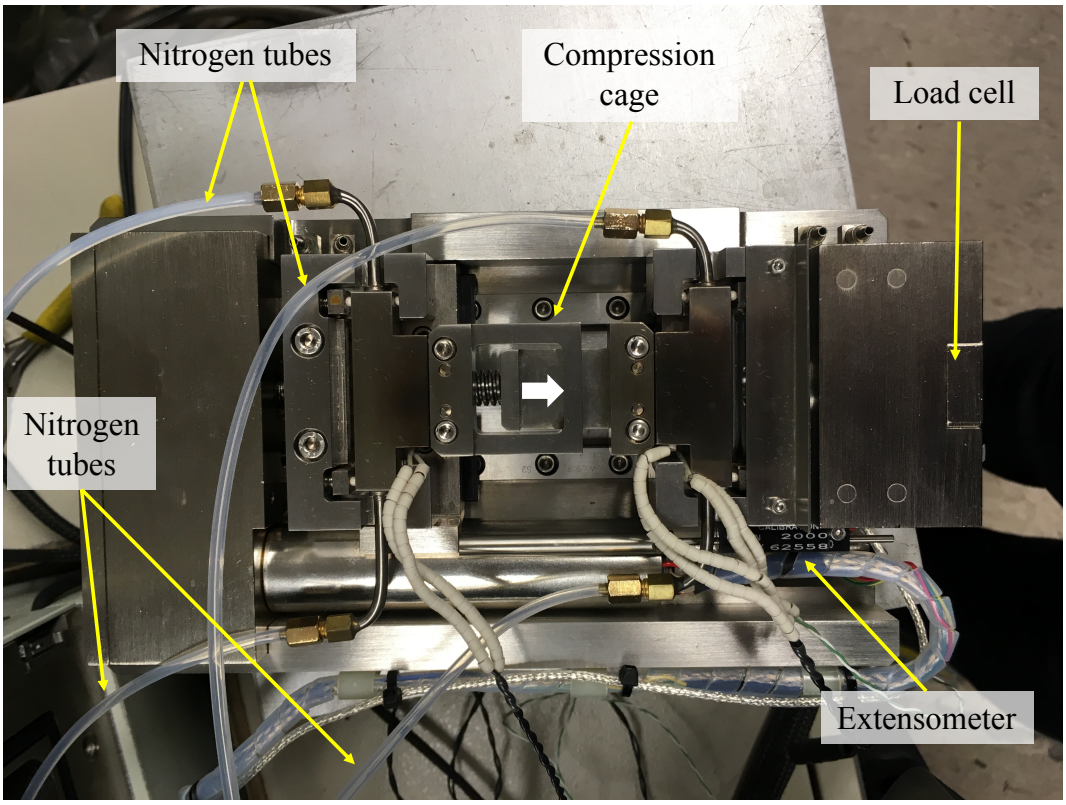

Figure 1: Components of the Deben Microtest deformation stage for a compression test. The sample is placed inside the compression cage, with the load applied in the direction indicated by the white arrow

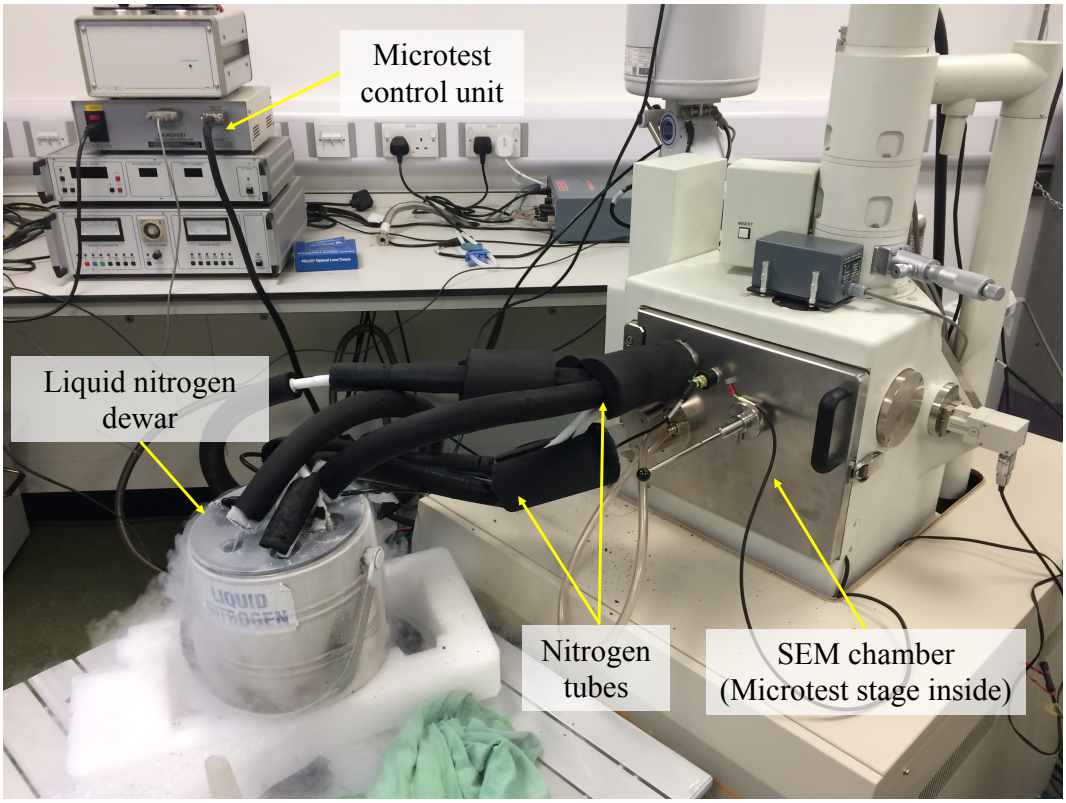

Figure 2: Experimental set-up used in these tests. The Microtest stage is placed inside the chamber of the SEM and cooled via the circulation of supercooled nitrogen gas.

Sample Preparation

The samples used in the preliminary tests were made in the cold rooms of the UCL Ice Physics Laboratory. For these preliminary tests, the aim was not to produce samples with a controlled microstructure, but rather to create 'dummy' samples with minimal preparation time, but with reproducible dimensions. This was done so that the number of tests conducted over the four-day period could be maximised. However, as will be discussed later, it should be noted that future tests will utilise ice samples with a tightly controlled microstructure. It should also be noted that, in contrast to some previous SEM studies [e.g. *Mulvaney et al.,* 1988; *Wolff et al.*, 1988], the samples were not coated to prevent charging as the SEM used is a variable pressure instrument and coating is unnecessary.

The desired final dimensions of both level ice and freeze-bonded samples was 15×10×5 mm. Plastic sample replicas were 3D-printed and used to create silicone rubber moulds. Two types of mould were made – one rectangular for level ice samples, and one with a 45-degree cut at the centre to make each end of the freeze-bonded samples. In the case of the freeze-bonded samples, the aim was to create a freeze-bond plane at a 45-degree angle to the axis of compression, so that shear failure could occur. Using silicone rubber had the advantage of forming moulds that were flexible, so that the ice samples could be removed easily.

De-ionised water was placed into the moulds using a syringe and moved inside a cold room, which was set to a nominal air temperature of -15°C. Once frozen, the samples were carefully removed from the moulds using tweezers and stored in small sealable plastic bags. For the freeze-bonded samples, the two end sections of ice were frozen onto a microscope glass such to create contact with their 45-degree edges., as shown in Figure 3b. A few drops of de-ionised water at its freezing temperature were placed onto the contacting section and left to consolidate for one minute. A small amount of heat was then applied to the base of the microscope glass to remove the freeze-bonded sample. Images of level ice and freeze-bonded samples are shown in Figures 3a and 3b respectively.

Samples were transported as quickly as possible from the Ice Physics Laboratory to the SEM Laboratory in a small polystyrene box containing dry ice. Once inside the SEM Laboratory, samples were then stored inside a temperature-controlled freezer set to -15°C.

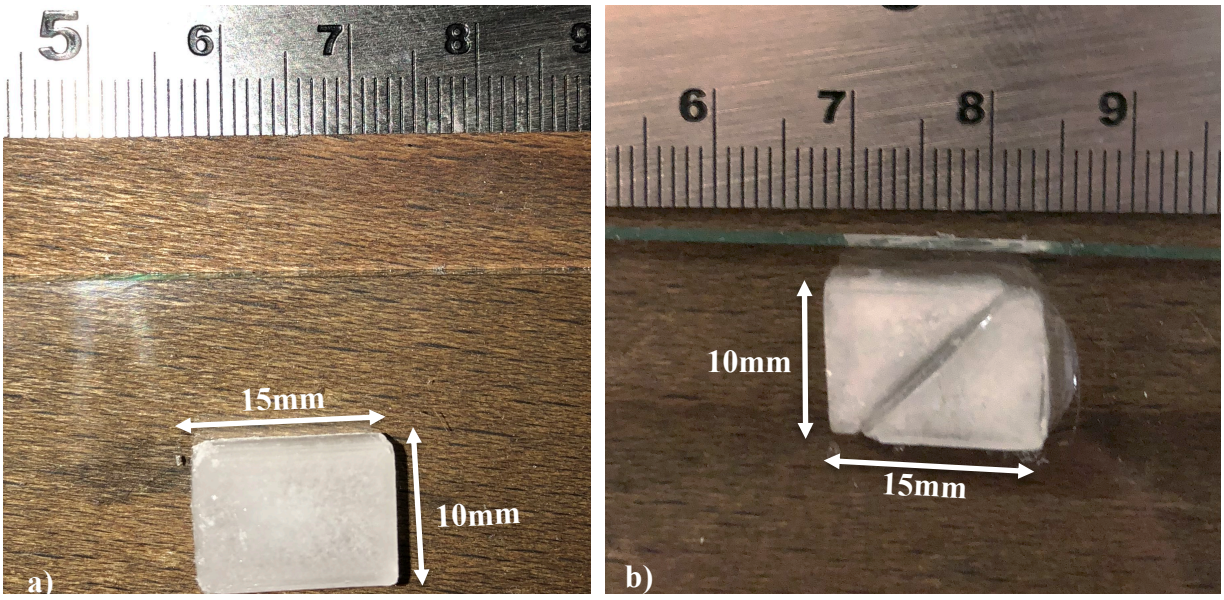

Figure 3: a) photograph of level ice sample, and b) photograph of freeze-bonded ice sample

RESULTS FROM PRELIMINARY TESTS

Six practice tests on dummy ice samples were conducted, the results of which are detailed in this section. It should be emphasised that the aim of these tests were not to obtain a set of high-quality results, but rather to enable proof of concept and to provide valuable practice for future, more controlled tests. Four level ice tests were conducted first, each at a different strain rate. Following this, two tests on freeze-bonded samples were conducted, both at a strain rate of 4×10^{-4} s^{-1}. The nominal test temperature for each test was –35 ± 2 °C. The low temperature was used to reduce the amount of sublimation from the samples, which may have resulted in damage to the SEM, as well as reduced quality of imaging.

Pre-Deformation Imaging

Prior to deformation, the surface of each sample was imaged on high-vacuum (secondary electron) mode, with the accelerating voltage varied between 4-15 kV. The accelerating voltage was varied over this range with the aim of determining the optimal value to achieve the highest quality imaging. Imaging the sample prior to deformation also enabled the temperature of the sample to equilibrate to the stage temperature. At the lowest magnitude (×10) the majority of the sample surface was in the field of view of the microscope.

Figures 4a and 4b show the typical surfaces of a level ice sample and freeze-bonded sample respectively. It should be noted that the surfaces of the other samples exhibited similar topographies to those shown in Figure 4. Observing first the level ice surface in Figure 4a, it can be seen that structural defects in the form of surface cracks are present in the sample, which probably resulted from the crude sample preparation. Additionally, a diagonal lined structure was visible on the surface of samples. This originated as a result of imprinting of the ice surface from the silicone rubber moulds during freezing, and was also observed under prior visual inspection.

Figure 4b shows the surface of a freeze-bonded sample. The surface of the freeze-bonded samples contains more surface structure as a result of freezing of water used to bond the two sections of the ice. In contrast to preceding visual inspections, no obvious freeze-bond layer was visible under the SEM. However, the position of the freeze-bond layer could be inferred by observing the region of raised topography approximately symmetric about an axis 45 degree to the length of the sample. This feature probably originated from the freezing of water which overflowed from the freeze-bond layer. An estimate for the position of the freeze-bond layer is shown in Figure 4b.

Upon further magnification, it was possible to observe the individual grains and accompanying grain boundaries in regions of several of the level ice samples. However, due to frost build-up it was not possible to observe grains in all level ice samples, and in the case of the freeze-bonded samples was not possible at all due to the presence of a recently frozen layer of ice on the surface resulting from the bonding procedure. A more controlled grain size is possible using other ice growth methods [e.g. *Cole*, 1979; *Vaughan et al.*, 2017] and will be utilized in future tests. Sublimation patterning was also visible at x100 magnification, which arose as a result of the high temperature used in these tests. These sublimation patterns are similar to those observed via etching in similar SEM observations [e.g. *Barnes et al.*, 2002; *Baker and Cullen*, 2003].

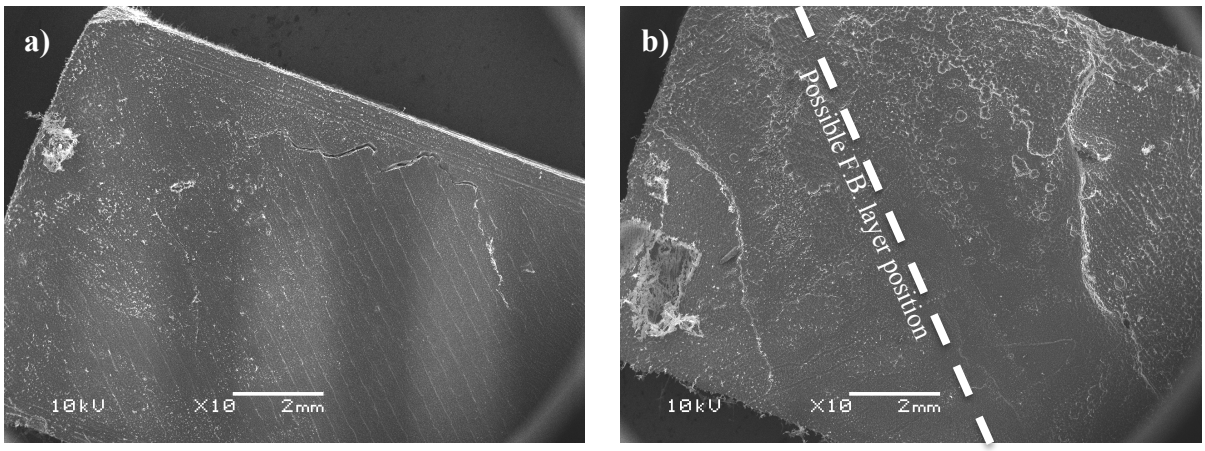

Figure 4: SEM images taken prior to deformation for a) level ice sample, and b) freeze-bonded (F.B.) sample

Compression Tests on Practice Ice Samples

Once the samples had been imaged and had been allowed to equilibrate with the stage temperature, compression tests were conducted and simultaneously imaged.

The failure mode for each test was deduced from the SEM imaging, and was greatly aided by the ability to video the deformation. Two types of failure mechanisms were observed: propagation of pre-existing cracks, and axial splitting. In the former case, the pre-existing crack propagated after the nominal strain exceeded approximately 0.8%. The crack propagation was clearly observed in the videoing, such is in Figure 5.

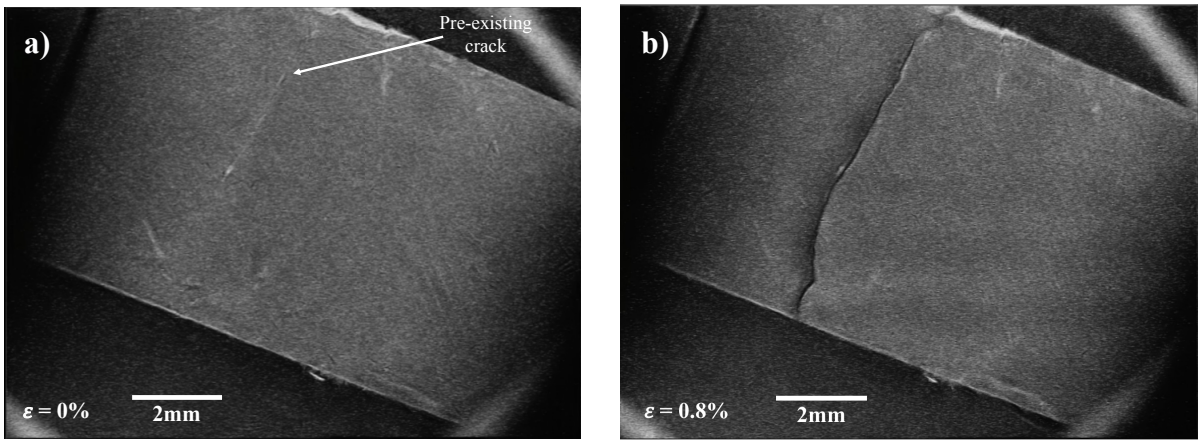

Figure 5: Propagation of pre-existing crack in sample used in Test 1, a) prior to crack propagation, and b) immediately after crack propagation

Axial splitting of samples was an observed failure mechanism in both level ice and freeze-bonded samples at the lower strain rates. In the level ice samples, the axial splitting was accompanied by shards, as shown in Figure 6a, whereas the freeze-bonded samples split into two distinct sections, as shown in Figure 6b. It should be noted that the freeze-bonded sample failed off-axis with the freeze-bond layer, which indicated that shear freeze-bond failure did not occur.

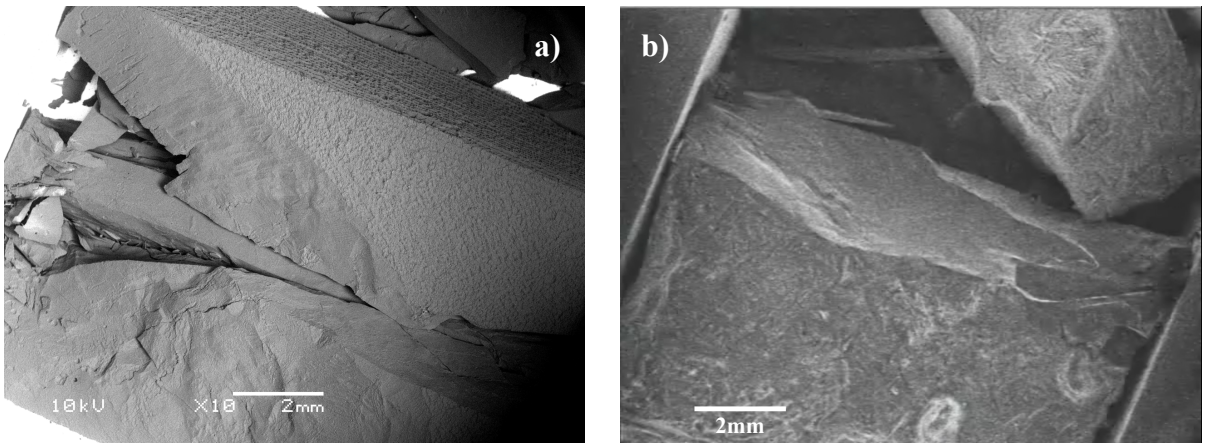

Figure 6: Failure via axial splitting in a) level ice sample, and b) freeze-bonded sample

The mechanical results obtained from each test are shown in Table 1. There was considerable variation in the measured compressive strength in the level ice samples, which was deduced from the stress-strain curves shown in Figure 7a. Overall the compressive strength varied from 1.84 MPa (Test 3) to 17.08 MPa (Test 4) and does not appear to exhibit any apparent relationship with strain-rate. The two failure modes yielded different values of compressive strength. The samples that failed via pre-existing crack propagation tended to be weaker. Thus, it should be noted that these strength values should not be compared, since different failure processes are occurring. Additionally, the stress-strain curves in Figure 7 exhibit varied shapes. Test 4, which was conducted at the lowest strain-rate, exhibits the most brittle stress-strain behavior.

Table 1. Mechanical parameters for each practice tests conducted. Two types of failure mode were observed: 'Crack Prop.'= propagation of pre-existing surface cracks, 'Axial Splitting'= longitudinal fracture of sample

Test No.	Ice Type	Strain Rate [s^{-1}]	Strength [MPa]	Failure Mode
1	Level Ice	2×10^{-3}	6.59	Crack Prop.
2	Level Ice	9×10^{-4}	1.84	Crack Prop.
3	Level Ice	4×10^{-4}	3.21	Axial Splitting
4	Level Ice	2×10^{-5}	17.08	Axial Splitting
5	Freeze-Bonded	4×10^{-4}	2.05	Axial Splitting
6	Freeze-Bonded	4×10^{-4}	1.64	Axial Splitting

The two freeze-bonded tests (Test 5 and Test 6) were conducted at the same strain rate of 4×10^{-4} s^{-1}, and the resulting stress-strain curves are shown Figure 7b. In Test 5, the sample failed at 2.05 MPa, and in Test 6, the sample failed at 1.64 MPa. Despite the similar test conditions, and freeze-bond contact time, the sample in Test 5 was 500 KPa stronger, which may be attributed to a difference between the initial structure of the ice, or a difference in the volume of liquid used to bond the pieces of ice. Both freeze-bonded samples were weaker than the level ice test conducted at the same strain rate. Compared to the level ice tests, the

stress-strain behaviour is more jagged, and does not exhibit a clear elastic region. The stress-strain relationship is reminiscent of stick-slip behaviour observed in friction experiments on ice.

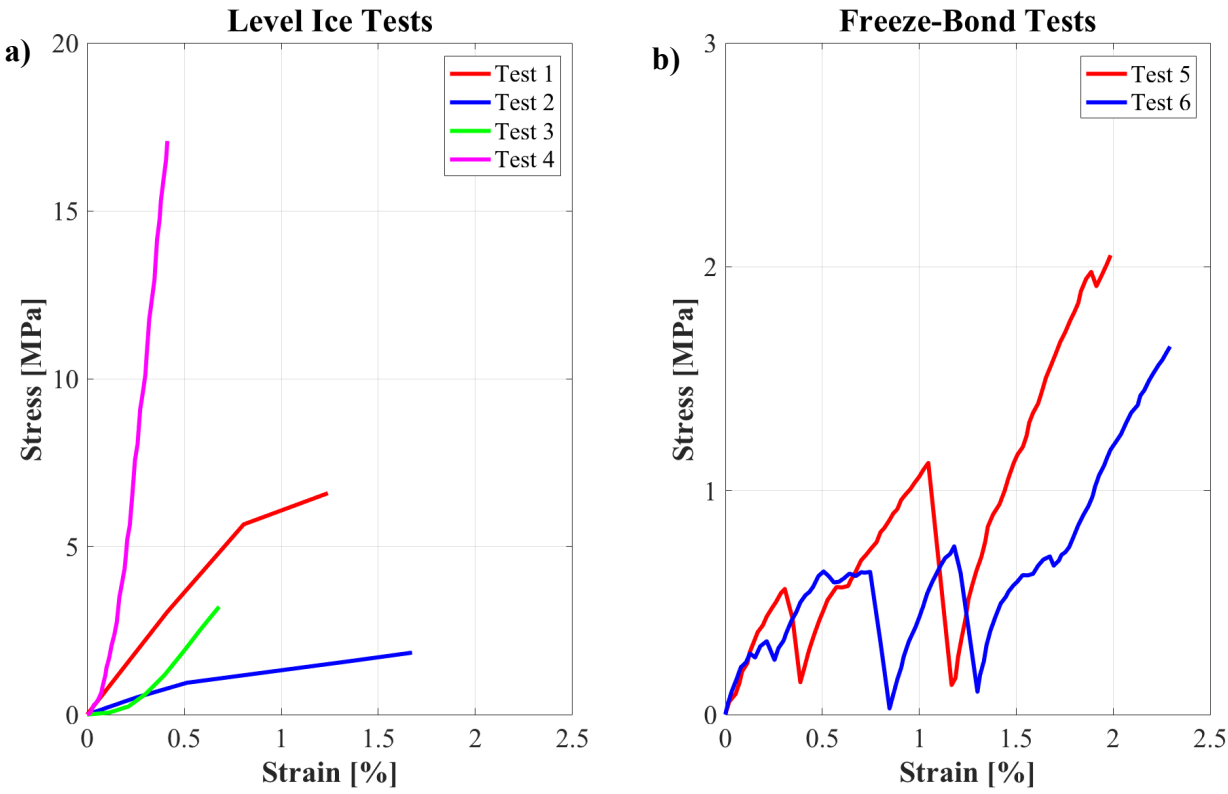

Figure 7: Stress-strain curves for a) level ice tests, and b) freeze-bonded ice tests

DISCUSSION

There was considerable range in the measured compressive strength of the level ice samples. The observed stress-strain curves and imaging indicate that the level ice tests were brittle in nature. Quoted values for the brittle unconfined compressive strength of fresh polycrystalline ice exhibit strong temperature and strain-rate dependencies. *Carter* (1971) conducted unconfined compression tests on fresh granular ice samples at -32°C and at strain-rates between 10^{-3} to 10^{-1} s^{-1}. At the lowest strain rates (comparable to our tests), they measured an unconfined compressive strength of ~17 MPa, which is comparable to the strength result obtained in Test 4. The strength measured in Test 4 is also similar to results obtained by *Schulson* (1990) for brittle compressive strength of fresh granular ice over a similar temperature range. *Rist and Murrell* (1994) also observed high failure stresses at comparable temperatures and strain rates during triaxial tests on freshwater polycrystalline ice samples. However, it should be noted that our tests were conducted on a smaller spatial scale to the results from *Carter* (1971), *Schulson* (1990) and *Rist and Murrell* (1994) so direct comparison of results may not be appropriate due to scaling effects.

However, this does not address the fact that three of the four level ice samples (Samples 1,2,3) exhibited significantly weaker compressive strengths. This is probably due to the presence of structural defects (i.e. cracks) in these samples existing prior to deformation. This is supported by observations of failure modes in Test 1 and Test 2, both of which failed via

propagation of pre-existing cracks. Test 3 did not appear to fail via the same mode, but it is possible failure may have resulted due to the propagation of cracks existing deeper in the sample which could not be visible at the imaged surface. Weakening of the ice due to the presence of damage in the samples is supported by *Timco* (1987), who suggested that a damage threshold above which the compressive strength decreases. If this were the case, it would indicate that samples in Tests 1, 2 and 3 exceeded the damage threshold, whilst the sample in Test 4 did not.

Axial splitting of the level ice samples was a frequently observed failure mode, and commonly occurs in deformation of ice under compression [e.g. *Cannon et al.*, 1990]. The imaging in the two freeze-bond tests indicated that failure occurred via splitting approximately along the direction of loading, suggesting that full shear failure of freeze-bonds did not occur. The failure modes were more reminiscent of the compressive failure occurring in Test 4. This may be because the samples had completely consolidated prior to the start of deformation. In this case, the freeze-bonds may have been as strong, or even stronger than the surrounding level ice, similar to that observed in *Høyland and Møllegaard* (2014). However, a different conclusion may be drawn from the stress-strain curves for the freeze-bond tests. As mentioned, in both cases the stress-strain data exhibited a jagged shape reminiscent to stick-slip in friction tests. This would suggest that the freeze-bonded samples failed in shear rather than compression.

A full characterisation of the failure modes remains a major challenge in this research. Even when videoed, it was difficult to deduce processes occurring instantaneously during the deformation. This is not helped by the currently obtained resolution of the videoing, which is low when compared to individual images. Additionally, as demonstrated in the freeze-bond tests, it is difficult to link the stress-strain data to the failure modes deduced from imaging. Ideally, it would be desirable to establish auto-capturing of images at a high sampling frequency, so that a higher resolution video could be obtained. However, this is currently not possible using our SEM, as the fastest sampling interval is approximately 20 seconds.

One important question that must be addressed: what is the ideal test temperature? There is a trade-off between the optimal conditions for imaging and the conditions comparable to those encountered in the field. To minimise significant levels of sublimation during testing, the sample temperature should be kept below -130°C [*Barnes et al.*, 2002] which is significantly below ice temperatures encountered in the field. The temperature used in these tests was comparatively high, and was chosen both to enable comparison with field conditions, as well as to reduce nitrogen consumption (which was limited in these tests) and time required to cool the Microtest stage. This was at the expense of optimal imaging conditions, and significant levels of sublimation from the sample occurred.

Despite a high test temperature compared to other SEM studies on ice, it was still lower than typically found in the field, which makes representative testing difficult since the mechanical properties of ice are highly temperature dependent. This is particularly relevant for the tests on freeze-bonded ice. In a ridge keel, the freeze-bond temperature will vary from the freezing temperature in the unconsolidated rubble region, to around the local level ice temperature in the consolidated layer, which is usually higher than the test temperature used in these tests. This is similarly the case in the consolidation of rafted layers of sea ice, where the freeze-bond temperature would be expected to approach the midpoint between the local atmospheric temperature and the freezing point if we assume simple rafting between two floes of uniform thickness [*Bailey et al.,* 2012]. Therefore, future SEM tests on freeze-bonded ice samples will focus on obtaining the temperature dependency, with the test temperature described here used as the lower bound. This would enable acquisition of data at ice temperatures representative of field conditions, as well as at the lower temperatures preferable for higher quality imaging.

CONCLUSIONS

In this paper we have described the methodology for in-situ deformation of millimetre-scale ice samples under a scanning electron microscope. We have also summarized results from preliminary compression tests on dummy samples over a range of strain rates. Both level ice and freeze-bonded samples were used. Prior to deformation, each sample was imaged under the SEM, revealing surface features such as grain boundaries and sublimation patterning. Stress-strain curves were obtained, and the deformation was imaged real-time so that the micromechanical processes and eventual failure modes could be deduced.

The level ice samples exhibited brittle-type behaviour, with compressive strength ranging between 1.94-17.08 MPa, and did not exhibit any apparent strain-rate dependency. However, we believe only the test with the highest compressive strength (Test 4) to be representative of the true mechanical behaviour of ice. In this case, the sample failed via axial splitting. Weaker samples tended to fail via propagation of pre-existing cracks in the sample, which was clearly visible in the imaging. It is unclear as to whether the freeze-bonded samples failed via shearing along the layer. The SEM imaging indicated that the samples failed in compression via axial splitting. However, the stress-strain behaviour in both freeze-bond tests was somewhat reminiscent of stick-slip occurring in shear failure. Full determination of the failure modes remains a major challenge in this research. In either case, it is almost certain that the samples had completely consolidated and had reached a strength comparable or even greater than the surrounding level ice.

The results from these preliminary tests highlight the necessity for tightly controlled, defect-free samples, if comprehensive analyses of micromechanical processes are to be conducted. Future tests will use fresh granular ice samples grown under controlled conditions, as well as laboratory-grown saline ice. It may also be desirable to use lower test temperatures than used in these tests to attain a higher quality of imaging. By conducting equivalent tests on larger scales, we aim to establish empirical scaling laws for the mechanical properties of ice.

ACKNOWLEDGEMENTS

We would like to thank Jim Davy for his assistance in conducting these tests, and for construction of the sample moulds. Thanks also to Gary Tarbuck, Andrew Thompson, Neil Hughes and Ernest Samuel for their technical support. We would thank the SAMCoT team for their valuable feedback on the described experimental methodology. The research was funded by an IRDR UCL Impact Studentship with SAMCoT.

REFERENCES

Bailey, E., Sammonds, P.R. & Feltham D.L., 2012. The consolidation and bond strength of rafted sea ice. *Cold Regions Science and Technology,* 83-84, pp. 37–48.

Baker I. & Cullen D., 2003. SEM/EDS observations of impurities in polar ice: artifacts or not?. *Journal of Glaciology*, 49(165), pp. 184-190.

Barnes, P.R.F., Mulvaney, R., Wolff., E.W. & Robinson, K., 2002. A technique for the examination of polar ice using the scanning electron microscope. *Journal of Microscopy*, 205, pp. 118-124.

Cannon, N.P., Schulson, E.M., Smith, T.R., Frost, H.J., 1990. Wing cracks and brittle compressive fracture. *Acta Metallurgica et Materialia*, 38(10), pp. 1955-1962

Carter, D., 1971. *Lois et mechanismes de l'apparente fracture fragile de la glace de riviere et de lac*. Ph.D. University of Laval.

Cole, D. M., 1979. Preparation of polycrystalline ice specimens for laboratory experiments. *Cold Regions Science and Technology*, 1(2), pp. 153-159.

Cross, J.D., 1969. Scanning electron microscopy of evaporating ice. *Science*, 164, 174–175.

Ettema, R & J A Schaefer (1986). "Experiments on freeze-bonding between ice blocks in floating ice rubble". *Journal of Glaciology*, 32(112), pp. 397–403.

Høyland, K.V. and Møllegaard A., 2014. Mechanical behaviour of laboratory made freeze-bonds as a function of submersion time, initial ice temperature and sample size. In: *22nd IAHR International Symposium on Ice, Singapore, August 11 to 15, 2014*.

ISO/FDIS/19906, 2010. Petroleum and natural gas industries - Arctic offshore structures. International Organization for Standardization, Geneva, Switzerland.

Mulvaney, R., Wolff, E.W. & Oates, K. ,1988. Sulphuric acid at grain boundaries in Antarctic ice. *Nature*, 331, 247–249.

Repetto-Llamazares, A.H.V., Høyland, K.V. & Evers K-U., 2011. Experimental studies on shear failure of freeze-bonds in saline ice: Part I. Set-up, failure mode and freeze-bond strength. *Cold Regions Science and Technology,* 65(3), pp. 286–297

Rist, M.A. & Murrell, S.A.F, 1994. Ice triaxial deformation and fracture. *Journal of Glaciology*, 40(135), pp. 305-318.

Sammonds, P., Montagnat,, M., Bons, P. & Schneebeli, M., 2017. Ice microstructures and microdynamics. *Philosophical Transactions of the Royal Society A: Mathematical, Physical and Engineering Sciences*, 375(2086).

Schulson, E.M., Baker, I., Robertson, C.D., Bolon, R.B. & Harnimon, R.J., 1989. Fractography of Ice. *Journals of Materials Science Letters,* 8, pp. 1193-1194

Schulson, E.M., 1990. The brittle compressive fracture of ice. *Acta Metallurgica et Materialia*. 38(10), pp. 1963-1976.

Shafrova, S. & Høyland, K.V., 2008. The freeze-bond strength in first- year ice ridges. Small-scale field and laboratory experiments. *Cold Regions Science and Technology* 54(1), pp. 54–71.

Timco, G.W., 1987. Ice structure interaction tests with ice containing flaws. *Journal of Glaciology*, 33(114), pp. 186–194.

Vaughan M., Prior D., Jefferd M. et al., 2017. Insights into anisotropy development and weakening of ice from in situ P wave velocity monitoring during laboratory creep. *Journal of Geophysical Research: Solid Earth*. 122(9), pp. 7076-7089.

Weiss, J., 2001. Fracture and fragmentation of ice: A fractal analysis of scale invariance. *Engineering Fracture Mechanics*, 68(17-18), pp. 1975-2012.

Weiss, J. & Dansereau, V., 2017. Linking scales in sea ice mechanics. *Philosophical transactions. Series A, Mathematical, physical, and engineering sciences.* 375(2086).

Wolff, E.W., Mulvaney, R. & Oates, K., 1988. The location of impurities in Antarctic ice. *Annals of Glaciology*, 11, pp. 194–197.